An evaluation method for uncertainties in regional climate projections

Adachi, Sachiho A. ; Nishizawa, Seiya ; Ando, Kazuto ; Yamaura, Tsuyoshi ; Yoshida, Ryuji ; Yashiro, Hisashi ; Kajikawa, Yoshiyuki ;…

RESEARCH ARTICLE

An evaluation method for uncertainties in regional climate projections

Sachiho A. Adachi[1,2] 🄴 | Seiya Nishizawa[1] 🄴 | Kazuto Ando[1] | Tsuyoshi Yamaura[1] |
Ryuji Yoshida[1,3] 🄴 | Hisashi Yashiro[1] | Yoshiyuki Kajikawa[1,3] | Hirofumi Tomita[1,2]

[1]Computational Climate Science Research Team, RIKEN Center for Computational Science, Kobe, Japan

[2]Mathematical Climatology Laboratory, RIKEN Cluster for Pioneering Research, Kobe, Japan

[3]Research Center for Urban Safety and Security, Kobe University, Kobe, Japan

Correspondence
Sachiho A. Adachi, RIKEN Center for Computational Science, 7-1-26 Minatojima-minami-machi, Chuo-ku, Kobe 650–0047, Japan.
Email: sachiho.adachi@riken.jp

Present address
Ryuji Yoshida, CIRES, University of Colorado Boulder, Boulder CO, 80309.NOAA Earth System Research Laboratory, Boulder CO, 80305.

Regional climate projections inevitably inherit uncertainties from general circulation models (GCMs). We therefore propose a new approach for identifying the dominant uncertainties. This approach employs the downscaling procedure by Adachi et al. to the uncertainty problem using multiple GCM projections. The mean state of the large-scale atmospheric states and the deviation from this mean state are the two uncertainty factors considered here, which are provided by a GCM. These two factors are referred to as climatology and perturbation components, respectively. To demonstrate the effectiveness in identifying these uncertainty factors using the proposed approach, a regional projection of summertime climate in western Japan is conducted using four different future climate data that are calculated using an atmospheric GCM with different sea surface temperatures. Results show that the variability in surface air temperature projections is reasonably derived from the climatology uncertainty, whereas the variability in precipitation projections is equally influenced by the climatology and perturbation uncertainties. Both the climatology and perturbation uncertainties should therefore be considered when analysing regional climate projections.

KEYWORDS
dynamical downscaling, regional climate model, regional climate projection uncertainties, uncertainty evaluation

1 | INTRODUCTION

It is important to elucidate uncertainties that persist in regional climate projections when designing adaptation plans to anticipate future climate change. The sources of uncertainty in future climate projections are primarily divided into three categories (Hawkins and Sutton, 2009, 2011): internal variability, the greenhouse gas emission scenario and imperfections in general circulation models (GCMs). Uncertainty related to internal variability is present in the projections regardless of global warming and its influence decreases relative to climate change signal due to global warming when

longer prediction lead times are considered. Differences in the greenhouse gas emissions affect the radiative balance of the atmosphere. Uncertainties due to GCM imperfections occur because GCMs generally exhibit different climate sensitivities to certain external forces (e.g., greenhouse gases) and exhibit different spatial patterns in the atmospheric fields even if the global climate sensitivities are of the same degree. Uncertainties due to imperfections in regional climate models (RCMs) should also be considered in regional climate projections that employ downscaling simulations (Wilby and Dessai, 2010) because they can show different downscaled climates even if the RCMs use the same

boundary conditions and similar model configurations (e.g., domain and grid spacing).

Regional-scale comparisons of these uncertainties have been performed using multi-GCMs (e.g., Giorgi and Francisco, 2000; Hawkins and Sutton, 2011), multi-RCMs (e.g., Ishizaki *et al.,* 2012), multi-GCM/RCM combinations (e.g., van der van der Linden and Mitchell, 2009; Inatsu *et al.,* 2015; Sørland *et al.,* 2018) and a large number of ensemble simulations (Mizuta *et al.,* 2017). Hawkins and Sutton (2011) analysed multiple GCM projections and showed that the GCM model uncertainty was larger than the scenario uncertainty for both global and regional precipitation projections, except for the polar regions, at the end of 21st century. Inatsu *et al.* (2015) performed multi-model downscaling experiments with three GCMs and three RCMs and subsequently compared the uncertainty contributions derived from GCMs and RCMs to a regional climate projection. They showed that the downscaling results primarily depended on the GCM boundary conditions. A well-developed RCM for a target region has the advantages of reducing GCM climate biases and quantitatively modifying the GCM climate-change signals (Sørland *et al.,* 2018); however, an RCM still qualitatively inherits the tendency of the climate change signals projected by a GCM (e.g., Rowell, 2006; Déqué *et al.,* 2007). This study focuses on the uncertainties due to GCM projections in regional climate projections since GCM projection differences are one of the factors that lead to variations in regional climate projections.

Adachi *et al.* (2017) (henceforth, A2017) proposed a new downscaling procedure to quantitatively evaluate the contributions of three factors to regional climate change. A2017 basically used the same mathematical approach as the "factor separation method" proposed by Stein and Alpert (1993) and extended this approach to study regional climate projections. The three factors are the changes in two large-scale atmospheric components provided by a GCM, the climatology (mean state) and perturbation (deviation from the mean) components and the nonlinear effects between these two component changes. The thermodynamic and dynamic

TABLE 1 Examples and meanings of the climatology and perturbation changes from the viewpoints of thermodynamic and dynamic changes

	Thermodynamic change	Dynamic change
Climatology change	Increase in atmospheric moisture content due to warming temperatures (Clausius–Clapeyron relationship)	Changes in large-scale flow patterns associated with global circulation (e.g., width of the Hadley cell, position and strength of jets)
Perturbation change	Changes in temperature and specific humidity in the surrounding areas of a disturbance due to changes in the track of the disturbance	Changes in the frequency, intensity and track of the disturbances, such as tropical and extratropical cyclones

effects of these two component changes on regional climate are explained in A2017 and summarised in Table 1.

Here, we propose a new method for evaluating the uncertainties derived from GCM projections when assessing regional-scale projections. Specifically, we apply the procedure of A2017 to multiple GCM projections and evaluate how each of the three factors influences the variability in regional climate projections. Section 2 briefly introduces the concept and procedure of A2017 and then describes the experimental design of this study, along with the GCM climate data and the RCM employed here. The proposed method is then applied to summertime climate projections in western Japan (Section 3), with focus on surface air temperature and precipitation. Section 4 provides a summary and discussion of our results.

2 | METHODS

2.1 | Description of the principal concept and procedure

This subsection briefly introduces the procedure proposed by A2017, which is summarised in Figure 1a. Here we consider the changes in the large-scale atmospheric state between the present (p) and future (f) climates. We express p, which is provided by a GCM, as the sum of two components: the temporally averaged component, $\langle p \rangle$, and its deviation, p' such that $p = \langle p \rangle + p'$. We refer to the former and latter components as the climatology and perturbation components, respectively, following A2017. We similarly express f as $f = \langle f \rangle + f'$. These large-scale climate states are shown as diamonds on the climatology–perturbation phase space in Figure 1a, according to A2017 and Nishizawa *et al.* (2018), and they are used as RCM boundary conditions in our analysis. The vertical axis indicates the changes in a regional climate target variable that are estimated from downscaling experiments.

The regional climate change, Δ, is estimated from two direct dynamical downscaling (DDS) experiments, which are labelled PDDS (present DDS) and FDDS (future DDS) in Figure 1a. The boundary conditions for the DDS experiments are taken directly from the GCM output, with p for PDDS and f for FDDS.

Two additional downscaling experiments are conducted to extract the contributions of climatology and perturbation changes to regional climate, the pseudo climatology change downscaling (Pseudo-Clim-DS) and pseudo perturbation change downscaling (Pseudo-Perturb-DS) experiments. The boundary conditions for these experiments are prepared by altering either the climatology or perturbation component, where $\langle f \rangle + p'$ for the Pseudo-Clim-DS experiment and $\langle p \rangle + f'$ for the Pseudo-Perturb-DS experiment. The difference between the Pseudo-Clim-DS and PDDS experiments corresponds to the regional climate change due to
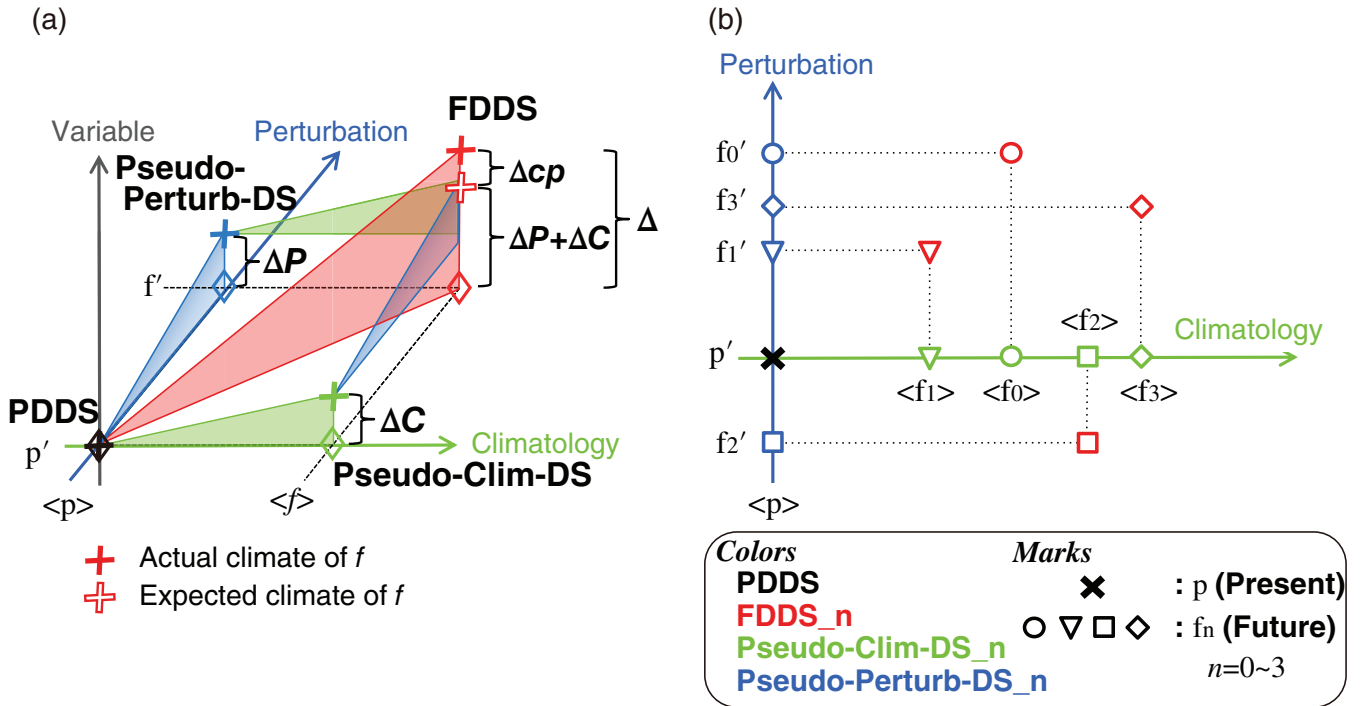
FIGURE 1 Schematics of the (a) basic downscaling procedure and (b) boundary condition relationships among the downscaling experiments conducted in this study. The subscript n ($n = 0 \sim 3$) uniquely identifies the future climate projections, which are calculated using MRI-AGCM3.2S with different SSTs. The experiments are the same as those described in Table 2. Note that the subscripts that identify the future climate projections are omitted in (a) because (a) illustrates the basic concept of the procedure proposed by A2017

climatology changes (ΔC), whereas that between the Pseudo-Perturb-DS and PDDS experiments corresponds to the regional climate change due to perturbation changes (ΔP).

We refer to the total regional climate change Δ as the actual climate change, with the sum of ΔC and ΔP representing the expected climate change. Therefore, the difference between the actual and expected climate changes corresponds to the nonlinear effect Δcp between ΔC and ΔP. This procedure allows us to estimate the total regional climate change between the two large-scale states, and then evaluate the contributions of these three factors on the total regional climate change: $\Delta = \Delta C + \Delta P + \Delta cp$.

2.2 | Experimental design for uncertainty evaluation

Here we apply the above procedure to evaluate the uncertainties derived from the boundary conditions. Although it is desirable to investigate the uncertainties using as many GCM projections as possible, it is not easy to obtain GCM outputs with the required temporal resolution for an RCM boundary condition. We therefore utilise one present climate and four future climate data from a single GCM for our uncertainty analysis. The details of these climate datasets and the GCM are described in following subsection.

When N sets of present and future climate datasets are available, $4N$ large-scale atmospheric states can be constructed. If a reference climate (i.e., present climate) is common for N future climates, $3N + 1$ large-scale atmospheric

states are constructed. Since one present and four future climate datasets are available in this study, we perform 13 downscaling experiments for our uncertainty analysis: one present climate DDS (reference state, PDDS), four future climate DDS (FDDS), four Pseudo-Clim-DS and four Pseudo-Perturb-DS experiments (Table 2). A conceptual diagram of the relationship between the boundary conditions for the 13 experiments is illustrated in Figure 1b.

TABLE 2 Experimental design for estimating the contributions of the changes in the climatology and perturbation components, and their nonlinearity to the variability in regional climate changes. DDS stands for direct dynamical downscaling. $\langle \rangle$ and $'$ indicate the climatology and perturbation components, respectively, of the large-scale boundary condition. p and f represent the present and future climate data, respectively, which are provided by MRI-AGCM3.2S. The subscript n ($n = 0 \sim 3$) uniquely identifies the future climate projections, which are calculated using different SSTs

Run name	Description of experiment	Boundary condition
PDDS	Present climate experiment via the DDS method	$\langle p \rangle + p'$
FDDS_n	Future climate experiment via the DDS method for future climate f_n	$\langle f_n \rangle + f_n'$
Pseudo-Clim-DS_n	Pseudo climatology change downscaling experiment for future climate f_n	$\langle f_n \rangle + p'$
Pseudo-Perturb-DS_n	Pseudo perturbation change downscaling experiment for future climate f_n	$\langle p \rangle + f_n'$

If we consider two DDSs (one PDDS and one FDDS), one Pseudo-Clim-DS and one Pseudo-Perturb-DS as a set of downscaling experiments, then N sets of experiments provide N sets of regional climate change information for Δ, ΔC, ΔP and Δcp. The difference between the estimated Δ values corresponds to the uncertainty in the regional climate projections estimated from multiple GCM projections. The variability among the estimated Δ values is broken into the variabilities derived from the climatology and perturbation components, which are estimated from the differences between the ΔC and ΔP values, respectively.

2.3 | Description of the GCM climate data and RCM model settings

Our method was applied to the changes in summertime precipitation and surface air temperature in western Japan to demonstrate its effectiveness in uncertainty evaluation. The climate data used as the RCM boundary conditions were provided by MRI-AGCM3.2S (Mizuta *et al.,* 2012), which is an atmospheric GCM. The present climate was simulated using a Hadley Centre Sea Ice and Sea Surface Temperature (SST) dataset (HadISST) (Rayner *et al.,* 2003) as forcing data. The four future climates were estimated using four different SSTs. The SST data for the future climates were constructed by summing the fluctuation, trend and climatological mean, and the climatological mean was further divided into the present climate and its future change (Mizuta *et al.,* 2008). The fluctuation was obtained from the HadISST dataset, which is the same as that for the present climate. The trend and future change of the climatological mean are obtained from the (a) multi-model mean of 28 coupled GCMs (CGCMs) under the RCP8.5 scenario, which are provided by the Coupled Model Intercomparison Project Phase 5 (CMIP5) (Taylor *et al.,* 2012), and (b) multi-model means for three model groups, classified using a cluster analysis of the dominant SST patterns among the

28 CGCMs (Mizuta *et al.,* 2014). Here, the future climate data, which are projected using the mean SST of the 28 CGCMs, are defined as f_0, whereas the others are labelled as f_1, f_2 and f_3. The present climate data are expressed as p.

The boundary conditions for the downscaling experiments are prepared using combinations of the climatology and perturbation components from the present and future climate datasets provided by MRI-AGCM3.2S, as shown in Table 2. Note that the specific humidity in the Pseudo-Clim-DS and Pseudo-Perturb-DS experiments is determined by the relative humidity in the present and future climates, respectively, where the relative humidity is assumed to be dependent on the perturbation component of each experimental climate. Therefore, the specific humidity for these experiments is calculated from the temperature, which is derived from the combination of the two components, and the relative humidity in the climate providing the perturbation component.

What does our investigation of the variability in downscaled climates due to differences in the climatology and perturbation changes mean? The difference in the experimental settings between the four MRI-AGCM3.2S future climate projections is the only forcing dataset on the SSTs. Our analysis therefore focuses on the regional climate projection uncertainties due to the GCM imperfections, which are recognised through the resultant SST patterns in the CMIP5 models.

The Scalable Computing for Advanced Library and Environment-Regional model (SCALE-RM) (Nishizawa *et al.,* 2015; Sato *et al.,* 2015; Yoshida *et al.,* 2017) was used to perform the downscaling experiments listed in Table 2, with the calculation domains shown in Figure 2a. The inner and outer domains are modelled using 2.5- and 7.5-km-grid intervals, respectively. The results from the inner domain, excluding lateral boundary nudging region, were used for the analysis. The physical schemes that are used in the experiments are listed in Table S1 of Appendix S1, Supporting Information. The calculation periods extend from June to
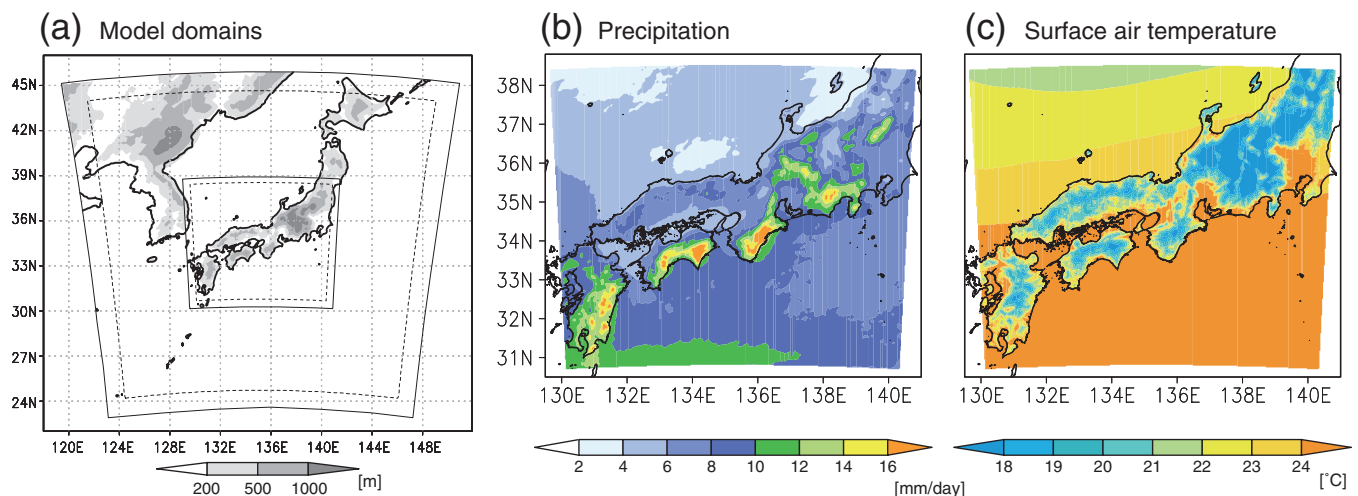

FIGURE 2 (a) Calculation domains and model topography, and PDDS distributions of the 25-year means of (b) precipitation and (c) surface air temperature at 2 m. The solid lines in (a) outline the entire calculation domains, with the dashed lines indicating the inner regions with no lateral boundary nudging region. The results in the inner region of the second domain are used for the analyses

September 1979–2003 for the present climate and from June to September 2075–2099 for the future climates. The 4-month downscaling simulation for each year is divided into 31 runs, with a run conducted every 4 days. The integration time of one run is 5 days, which includes 1 day for model spin-up. The PDDS precipitation and surface air temperature climatology is shown in Figure 2b,c, respectively. Their correlation coefficients are 0.85 and 0.92 for precipitation and temperature, respectively, based on 705 and 459 observation stations in the target region, respectively. The high degree of correlation between the observations and present climate model results indicates the sufficient model performance to demonstrate the proof-of-concept for evaluating the uncertainties in future regional climate projections.

3 | RESULTS

The predicted future changes (Δ) between the PDDS and four FDDS experiments are shown in Figure 3. We use three indices of the surface air temperature at 2 m (T2) for the analysis: mean temperature, daily maximum temperature and number of tropical-night days as well as three precipitation indices: mean precipitation, maximum 1-day precipitation and maximum number of consecutive dry days. A tropical-night day is defined as a day when the daily minimum T2 $\geq 20°C$, and a dry day is defined as a day when the daily precipitation <1 mm/day. All the indices are calculated in each year, and then temporally averaged over the 25-year period and spatially averaged across the analysis domain.

All the FDDS experiments indicate that the mean and daily maximum temperatures increase by 3.5–4.0°C in the future climates (Figure 3a,b). The number of tropical-night days also increases by 20 days per year (Figure 3c). The common trend among the three temperature indices is that the difference between the four projections, which is shown as |Max–Min| in each panel, is smaller than the future change in each instance. However, the precipitation results differ from the T2 results. The mean precipitation is projected to decrease in each future climate (Figure 3d), whereas each
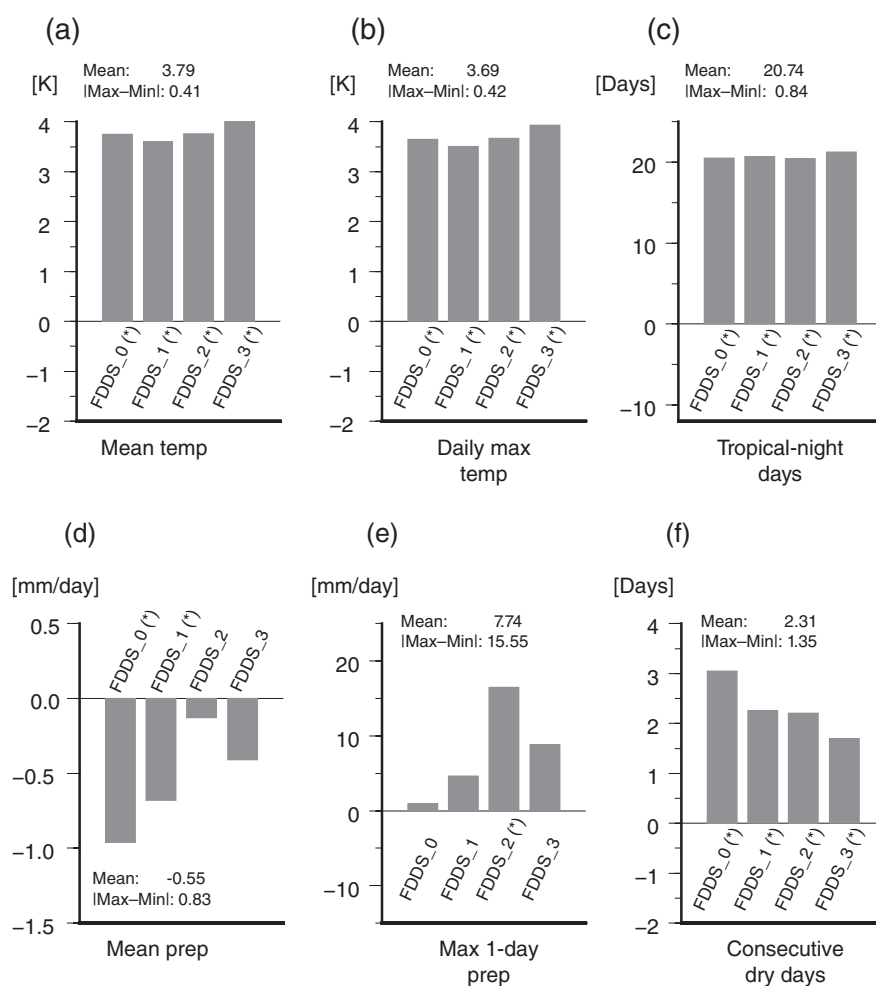

FIGURE 3 Differences between the PDDS and four FDDS precipitation and surface air temperature indices: 25-year-means of (a) surface air temperature, (b) daily maximum temperature, (c) tropical-night days, (d) daily precipitation, (e) maximum 1-day precipitation and (f) maximum consecutive dry days. A tropical-night day is a day when the daily minimum surface air temperature $\geq 20°C$, and a dry day is a day when the daily precipitation <1 mm/day. The asterisks after the experimental name indicate that the difference is statistically significant within the 95% confidence level. The "mean" in the panels indicates the mean value of the four projections, whereas "|Max-Min|" indicates the difference between the maximum and minimum values among the four projections

projection shows an increase in the maximum 1-day precipitation. The common trend among the two precipitation indices is that the spread of the four downscaled projections, shown as |Max-Min|, is larger than the absolute value of mean future change. Each future climate predicts an increase in consecutive dry days, with the spread of the four projections being smaller than the mean future change. These results imply that a single regional climate projection is insufficient to yield a statistically reliable projection, especially for precipitation, as suggested in previous studies (e.g., Rowell, 2006; Déqué *et al.*, 2007).

The contributions of each component in a large-scale atmospheric state to the variability in future climate changes are shown in Figure 4. Each mark in Figure 4 corresponds to its respective future projection in Figure 1b, with the exception that results are shown as the differences from the PDDS experiment (Δ, ΔP and ΔC). Each bar represents the mean of the four downscaling experiments. The Δ values (red symbols) are a condensed representation of the Figure 3 results.

The results for the three temperature indices (Figures 4a–c) show that Δ is primarily influenced by ΔC. The spread in the four Δ values of the mean and daily maximum temperature indices is also influenced by the variability in ΔC because the variance in ΔC is larger than that in ΔP. The variabilities in ΔC and ΔP are within the same range for the tropical-night days. These results show that the difference in

climatology projected by a GCM has a larger influence than the difference in perturbation on the downscaled temperature change and its variability in the climate projections.

The precipitation results show a completely different trend compared to the temperature results. The decrease in mean precipitation (Δ) is primarily explained by the precipitation decrease due to the perturbation changes (ΔP) in the four experiments. ΔP and ΔC exhibit the same degree of spread, and therefore equally influence the variability in Δ for mean precipitation. The spread in Δcp is smaller than that in the other two factors, but it is not negligible. The precipitation increase due to ΔC is generally larger than that due to ΔP for the maximum 1-day precipitation, yielding a projected increase in Δ. As with mean precipitation, both ΔP and ΔC provide similar contributions to the variability in Δ for the maximum 1-day precipitation, and Δcp is not negligible. The influence of ΔP and its variability is large compared to that of ΔC for the consecutive dry days, with the spread in Δ primarily due to the difference in ΔP. Our results therefore show that the main factor controlling future regional climate and its variability is not always the climatology of a GCM, as perturbation differences can also exert a strong influence on regional climate projections.

All four FDDS simulations yield a decrease in mean precipitation, which is primarily attributed to ΔP. A2017 explained the negative ΔP in mean precipitation for the Pseudo-Perturb-DS_0 experiment as a drastic decrease in
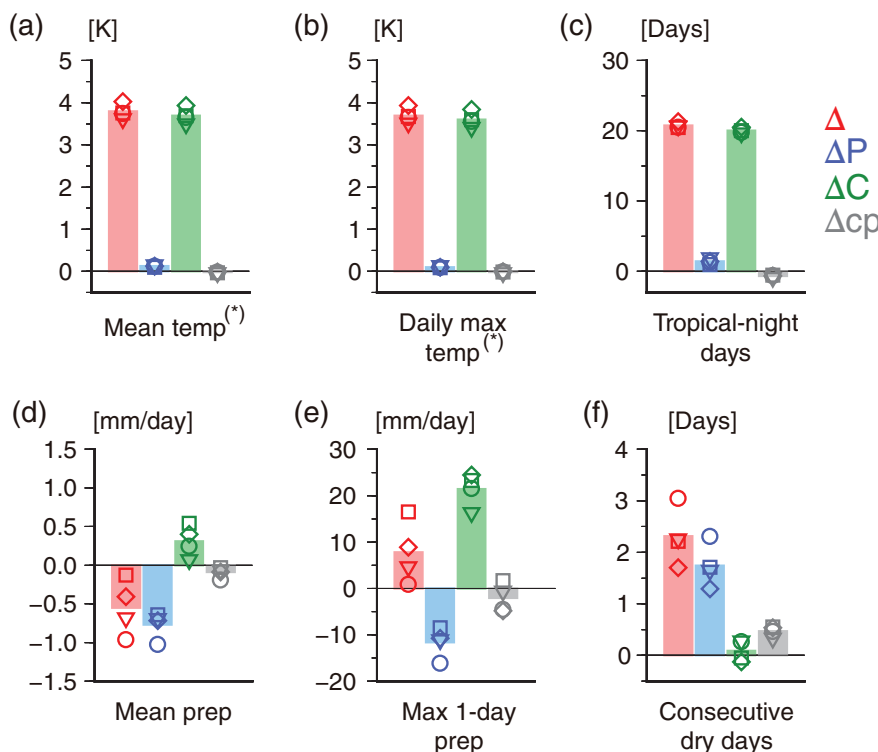

FIGURE 4 Variability among the future climate projections for the precipitation and surface air temperature indices. The indices are the same as those shown in Figure 3. Each mark represents an individual future projection and corresponds to its respective projection in Figure 1b. Δ is the total change estimated from the PDDS and FDDS experiments. ΔP and ΔC indicate the perturbation and climatology change contributions, respectively. Δcp is the contribution of the nonlinear effect between the two component changes. The evaluation indices with asterisks indicate that the variance of ΔC is larger than the variance of ΔP within a 95% confidence level

precipitation associated with typhoons. Here, we apply the same analysis to other cases and observe that the changes in precipitation associated with typhoons account for more than 60% of ΔP for all the Pseudo-Perturb-DS experiments. To determine the reason for the changes in ΔP that are associated with typhoons, we analysed the results from the viewpoint of the changes in event frequency and precipitation intensity of an event. We assumed that the precipitation (R) can be decomposed into the number of events (E) and mean precipitation intensity (I) of an event, where $R = E \times I$. Here we note that "precipitation intensity" is not an exact representation of the cyclone intensity but rather its impact on the target area. Given that $R = E \times I$ and $R' = E' \times I' = (E + \Delta E)(I + \Delta I)$ for the PDDS and Pseudo-Perturb-DS experiments, respectively, the precipitation change ($\Delta R = R - R'$) can be approximated as $\Delta R \sim \Delta E \times I + E \times \Delta I$, where $\Delta E \times I$ and $E \times \Delta I$ represent the influences due to the changes in the number of events and the changes in the precipitation intensity, respectively. We find that the primary factor for the changes in ΔP is due to the changes in the number of typhoons, that is, $\Delta E \times I$ of typhoons. On the other hand, the increase in mean precipitation due to ΔC is determined by the balance between the increase in precipitation associated with typhoons and non-typhoon cyclones, and the decrease in precipitation associated with other rain events. The former can be explained by rich moisture in the atmosphere due to soaring temperatures under the assumption of the same relative humidity, with the latter explained by the stabilisation of the atmosphere in the future climate.

4 | CONCLUSIONS AND DISCUSSION

We propose a new method to evaluate the uncertainties derived from GCM boundary conditions in regional climate projections by extending the procedure introduced by A2017. We consider the climatology and perturbation differences of the GCM projections as uncertainty sources. Our results show that the primary factor that influences the spread of future climate projections is the climatology component for surface air temperature indices, whereas it is the perturbation component for the consecutive dry days. For the mean and maximum 1-day precipitation indices, both the climatology and perturbation components are equally important factors. Improving the reliability of both the climatology and perturbation responses in a GCM is important for obtaining more accurate projections of regional climate change, especially for quantities with large nonlinearities such as precipitation. Therefore, considering both climatology and perturbation uncertainties on large-scale future climate projections are necessary when assessing future regional climate.

GCMs generally comprise different numerical schemes, especially for physical processes, and exhibit different responses to certain external forcings. Because the demonstration in this study used climate data produced by a single GCM, many experimental conditions are common among the four future climates such as the modelled climate response, model schemes, greenhouse gases and ground surface condition. We therefore consider our estimated variability in the downscaled climate projections to represent only a portion of those estimated using multiple climate projections from multiple GCMs. The proposed method needs to be applied to multiple future climate projections from different GCMs to properly assess the influences of these two components. Such results would improve our understanding of the uncertainties derived from GCM projections for the regional climate projections of a target region and provide valuable information on the regional climate itself.

CONFLICTS OF INTEREST

The authors declare no potential conflict of interests.

ORCID

Sachiho A. Adachi https://orcid.org/0000-0002-3066-6175
Seiya Nishizawa https://orcid.org/0000-0001-9457-7457
Ryuji Yoshida https://orcid.org/0000-0003-3238-2595

REFERENCES

Adachi, S.A., Nishizawa, S., Yoshida, R., Yamaura, T., Ando, K., Yashiro, H., Kajikawa, Y. and Tomita, H. (2017) Contributions of changes in climatology and perturbation and the resulting nonlinearity to regional climate change. *Nature Communications*, 8, 2224.

Déqué, M., Rowell, D., Lüthi, D., Giorgi, F., Christensen, J., Rockel, B., Jacob, D., Kjellström, E., de Castro, M. and van den Hurk, B. (2007) An intercomparison of regional climate simulations for europe: assessing uncertainties in model projections. *Climate Change*, 81, 53–70.

van der Linden, P. and Mitchell, J. F. B. (2009) *ENSEMBLES: Climate change and its impacts: Summary of research and results from the ENSEMBLES project.* Technical report, Met Office Hadley Centre, FitzRoy Road, Exeter, EX1 3PB, U. K.

Giorgi, F. and Francisco, R. (2000) Evaluating uncertainties in the prediction of regional climate change. *Geophysical Research Letters*, 27, 1295–1298.

Hawkins, E. and Sutton, R. (2009) The potential to narrow uncertainty in regional climate predictions. *Bulletin of the American Meteorological Society*, 90, 1095–1107.

Hawkins, E. and Sutton, R. (2011) The potential to narrow uncertainty in projections of regional precipitation change. *Climate Dynamics*, 37, 407–418.

Inatsu, M., Sato, T., Yamada, T.J., Kuno, R., Sugimoto, S., Farukh, M.A., Pokhrel, Y.N. and Kure, S. (2015) Multi-gcm by multi-ram experiments for dynamical downscaling on summertime climate change in Hokkaido. *Atmospheric Science Letters*, 16, 297–304.

Ishizaki, N.N., Takayabu, I., Oh'izumi, M., Sasaki, H., Dairaku, K., Iizuka, S., Kimura, F., Kusaka, H., Adachi, S.A., Kurihara, K., Murazaki, K. and Tanaka, K. (2012) Improved performance of simulated Japanese climate with a multi-model ensemble. *Journal of the Meteorological Society of Japan*, 90, 235–254.

Mizuta, R., Adachi, Y., Yukimoto, S. and Kusunoki, S. (2008) *Estimation of the future distribution of sea surface temperature and sea ice using the cmip3 multi-model ensemble mean.* Tech. Rep. 56, Meteor. Res. Insti, http://www.mri-jma.go.jp/Publish/Technical/DATA/VOL_56/tec_rep_mri_56.pdf.

Mizuta, R., Yoshimura, H., Murakami, H., Matsueda, M., Endo, H., Ose, T., Kamiguchi, K., Hosaka, M., Sugi, M., Yukimoto, S., Kusunoki, S. and Kitoh, A. (2012) Climate simulations using MRI-AGCM3.2 with 20-km grid. *Journal of Meteorological Society of Japan*, 90A, 233–258.

Mizuta, R., Arakawa, O., Ose, T., Kusunoki, S., Endo, H. and Kitoh, A. (2014) Classification of CMIP5 future climate responses by the tropical sea surface temperature changes. *SOLA*, 10, 167–171.

Mizuta, R., Murata, A., Ishii, M., Shiogama, H., Hibino, K., Mori, N., Arakawa, O., Imada, Y., Yoshida, K., Aoyagi, T., Kawase, H., Mori, M., Okada, Y., Shimura, T., Nagatomo, T., Ikeda, M., Endo, H., Nosaka, M., Arai, M., Takahashi, C., Tanaka, K., Takemi, T., Tachikawa, Y., Temur, K., Kamae, Y., Watanabe, M., Sasaki, H., Kitoh, A., Takayabu, I., Nakakita, E. and Kimoto, M. (2017) Over 5,000 years of ensemble future climate simulations by 60-km global and 20-km regional atmospheric models. *Bulletin of the American Meteorological Society*, 98, 1383–1398. https://doi.org/10.1175/BAMS-D-16-0099.1.

Nishizawa, S., Yashiro, H., Sato, Y., Miyamoto, Y. and Tomita, H. (2015) Influence of grid aspect ratio on planetary boundary layer turbulence in large-eddy simulations. *Geoscientific Model Development*, 8, 3393–3419.

Nishizawa, S., Adachi, S.A., Kajikawa, Y., Yamaura, T., Ando, K., Yoshida, R., Yashiro, H. and Tomita, H. (2018) Decomposition of the large-scale atmospheric state driving downscaling: a perspective on dynamical downscaling for regional climate study. *Progress in Earth and Planetary Science*, 5, 2.

Rayner, N.A., Parker, D.E., Horton, E.B., Folland, C.K., Alexander, L.V., Rowell, D.P., Kent, E.C. and Kaplan, A. (2003) Global analyses of sea surface temperature, sea ice, and night marine air temperature since the late nineteenth century. *Journal of Geophysical Research*, 108(D14), 4407. https://doi.org/10.1029/2002JD002670.

Rowell, D.P. (2006) A demonstration of the uncertainty in projections of UKclimate change resulting from regional model formulation. *Climatic Change*, 79, 243–257.

Sato, Y., Nishizawa, S., Yashiro, H., Miyamoto, Y., Kajikawa, Y. and Tomita, H. (2015) Impacts of cloud microphysics on trade wind cumulus: which cloud microphysics processes contribute to the diversity in a large eddy simulation? *Progress in Earth and Planetary Science*, 2, 23. https://doi.org/10.1186/s40645-015-0053-6.

Sørland, S.L., Schär, C., Lüthi, D. and Kjellström, E. (2018) Bias patterns and climate change signals in gcm-rcm model chains. *Environmental Research Letters*, 13, 074017.

Stein, U. and Alpert, P. (1993) Factor separation in numerical simulations. *Journal of the Atmospheric Sciences*, 50, 2107–2115.

Taylor, K.E., Stouffer, R.J. and Meehl, G.A. (2012) An overview of CMIP5 and the experiment design. *Bulletin of the American Meteorological Society*, 93, 485–498.

Wilby, R.L. and Dessai, S. (2010) Robust adaptation to climate change. *Weather*, 65, 180–185. https://doi.org/10.1002/wea.543.

Yoshida, R., Nishizawa, S., Yashiro, H., Adachi, S.A., Sato, Y., Yamaura, T. and Tomita, H. (2017) CONeP: a cost-effective online nesting procedure for regional atmospheric models. *Parallel Computing*, 65, 21–31.

SUPPORTING INFORMATION

Additional supporting information may be found online in the Supporting Information section at the end of the article.